

# CMB and BBN constraints on evaporating primordial black holes revisited

---

Sandeep Kumar Acharya,<sup>a</sup> Rishi Khatri<sup>a</sup>

<sup>a</sup>*Department of Theoretical Physics, Tata Institute of Fundamental Research, Mumbai 400005, India*

*E-mail:* [sandeepkumar@theory.tifr.res.in](mailto:sandeepkumar@theory.tifr.res.in), [khatri@theory.tifr.res.in](mailto:khatri@theory.tifr.res.in)

ABSTRACT: We derive new CMB anisotropy power spectrum and BBN constraints for evaporating primordial black holes with mass between  $10^{11}$  g and  $10^{16}$  g by explicitly solving the electromagnetic particle cascades of emitted particles and the deposition of this emitted energy to the background baryon-photon plasma. We show that the CMB anisotropies can provide stronger constraints compared to BBN and CMB spectral distortions on black holes with masses as small as  $M_{\text{BH}} = 1.1 \times 10^{13}$ g, a slightly smaller mass than what has been considered in literature until now. We also show that, with more up-to-date data on abundances of deuterium and helium-3, BBN constraints are strengthened significantly. The abundance of these primordial black holes constrains the epoch of inflation  $\sim 40$  e-folds after the epoch constrained by the CMB observations.

## 1 Introduction

Primordial black holes (PBH) have recently gathered attention as an explanation of dark matter [1] in light of the discovery of gravitational waves from the merger of black holes with the mass of tens of solar mass [2]. Regardless of whether PBH form a dominant component of dark matter today, evidence for their existence at any time in cosmic history, in any mass range, would give great insight into the initial conditions and, in particular, the initial density fluctuations of the universe (for a recent summary of these constraints, see [3]). PBHs are formed in the radiation dominated era when the radiation pressure is not able to resist the gravitational collapse in overdense regions [4–7]. Mass of the black hole, produced in this scenario, is of the order of horizon mass [6, 8]. Due to formation at different epochs, mass of PBHs can vary from Planck mass relics to  $\sim 10^{10}$  times heavier than the mass of the Sun [3]. Although PBH formation with extended mass spectrum is likely [9, 10], we will restrict ourselves to monochromatic PBH mass function in this work so as not to restrict ourselves to a particular model. Since PBHs are formed due to early universe small scale fluctuations, their abundance today puts constraints on the initial power spectrum on small scales [11, 12]. Therefore, deriving accurate constraints on the allowed abundance of PBHs through various cosmological probes is a subject of great interest today. In this paper, we calculate constraints on the allowed abundance of PBHs in the mass range  $\sim 10^{11} - 10^{17}$ g from CMB (Cosmic Microwave Background) anisotropy power spectrum, CMB spectral distortions and BBN (Big bang nucleosynthesis). There are constraints on accreting solar mass black holes in the early universe from CMB spectral distortions and CMB anisotropy power spectrum [13–15] but we will not consider them here.

Injection of energetic electrons, positrons and photons around the recombination era (at redshift  $z \sim 1000$ ) can heat the background baryon-photon plasma or, if the injected particles are sufficiently energetic ( $> 10.2$  eV), they can excite and ionize neutral hydrogen and helium. Additional ionizations due to extra energy injections lead to a higher freeze-out free electron fraction at the end of the recombination epoch ( $z \lesssim 1000$ ) as compared to the standard recombination history [16, 17]. Increased scattering of CMB photons with free electrons leads to the damping of the CMB temperature anisotropy power spectrum and a boost in the polarization on large scales [18–22]. Electromagnetic energy injection at  $z \lesssim 2 \times 10^6$  into the baryon-photon fluid results in  $y, i$ , and  $\mu$ -type spectral distortions (collectively called *yim* distortions hereafter) in the non-relativistic theory [23–30]. Recently, it has been shown that for energy injection at  $z \lesssim 2 \times 10^5$ , relativistic effects are important [31, 32]. At  $z > 2 \times 10^6$ , photon number non-conserving processes establish a Planck spectrum and erase any CMB spectral distortions [24, 28, 33, 34]. Energetic photons above the photo-dissociation threshold of deuterium and helium-4 can change the abundances of deuterium, helium-3 and helium-4 [35–42]. These energetic photons are efficient in photo-dissociating nuclei upto a redshift at which the pair-production threshold on the CMB photons is of the same order as the photo-dissociation threshold of the nuclei [40–42]. Above this critical redshift,  $z \approx 3 \times 10^6$  for helium-4 destruction and  $z \approx 3 \times 10^7$  for deuterium destruction,

constraints become exponentially weak as most of the energy is lost to pair-production on the CMB photons instead of destruction of BBN elements [38, 40].

Black holes emit energetic particles by Hawking evaporation [43, 44]. The effect of PBH evaporation on the CMB anisotropy power spectrum was studied in [45–47]. The authors in [45] only considered energy deposition from primary electrons, positrons and photons and neglected the decay products of heavier particles. Also, they ignored the evolution of energy spectra during black hole evaporation. The authors of [46] derived constraints for PBH in mass range  $10^{15} - 10^{17}$ g with 6 cosmological parameters [48] fixed. The authors in [47] provided CMB anisotropy constraints for monochromatic PBHs, taking into account secondary photons, electron-positron pairs after hadronization from quarks and gluons. For the energy deposition of high energy electromagnetic particles to the background medium, the authors of [45–47] used the result of [49]. Similar analysis was performed in [50] but with on-the-spot approximation which means that any energy injected at a particular redshift is deposited to the background baryon-photon fluid at that particular redshift. The low optical depth of high energy gamma rays [21] implies that the energetic photons deposit their energy gradually over an extended period of time. The authors in [51] derived constraints for PBHs in the mass range  $10^{15} - 10^{17}$ g without the on-the-spot approximation and using the result of [49]. It was recently shown that some of the energy inject even at  $z \sim 10000$  can survive until recombination and have an observable effect on the CMB anisotropy power spectrum [52]

In this paper, we derive CMB anisotropy constraints using our own recent calculations [52], by evolving the electromagnetic cascades in the expanding universe without assuming on-the-spot approximation. We extend the CMB anisotropy constraints to lower PBH mass or PBH decaying at higher redshifts upto the point at which the CMB anisotropy constraints are not competitive with the constraints from CMB spectral distortions and BBN. We find that the CMB anisotropy constraints are competitive for PBH mass  $\gtrsim 1.3 \times 10^{13}$ g, a slightly lower mass threshold than [47]. We also provide BBN constraints with a more up-to-date analysis of electromagnetic cascade with Hubble expansion taken into account [52] and obtain stronger constraints compared to [8, 53]. Our aim in this paper is to provide more accurate constraints from CMB probes and BBN. We like to point out that other cosmological signals like the global 21 cm signal [54] and astrophysical probes like gamma rays [55, 56], cosmic rays [57], 511 keV gamma rays line from galactic center [58–60] can give competitive or stronger constraints at the higher end of the mass range constrained by the CMB anisotropies.

We use Planck [48] cosmological parameters in all calculations.

## 2 Energy deposition from electromagnetic cascade

A high energy injected particle can boost a background electron or photon to a higher energy in a relativistic scattering. This boosted particle along with the original particle (with reduced energy compared to the original energy) can boost more background particles, creating more relativistic particles and thus causing an electromagnetic cascade. The average energy of

a particle in the cascade decreases as more energetic particles are produced. In an ionized universe, these particles can only heat the background electrons. For a partially neutral medium, sub-keV photons can photo-ionize and excite neutral atoms. Electrons and positrons with energy  $\gtrsim$ keV boost the CMB photons through inverse Compton scattering (IC). Photons below the Lyman-alpha threshold ( $=10.2$  eV) escape. For electrons and positrons, the energy loss rates are much faster compared to the Hubble rate [21, 31]. Therefore, electrons and positrons lose their energy instantaneously through IC to the CMB photons or as heat to background electrons. The energy loss rate of photons is comparable to the Hubble rate. Therefore, we have to evolve the photon spectrum with all the relevant scattering processes in an expanding universe. For such calculations, we have followed the approach of [21, 61, 62]. Our calculation of energy deposition of electromagnetic particles to background medium is detailed in [52]. The basic algorithm to evolve the cascades is following. We divide the energy range from  $\sim$ eV to  $\sim$ TeV in 200 log spaced energy bins. A particle, in a particular energy bin, after depositing a fraction of its energy to the background particles can only drop down to lower energy bins. Therefore, the information of subsequent electromagnetic cascade of lower energy particles can be used to calculate to full cascade evolution history of original injected particle. Starting from lowest energy bins with energy of the order of few eV, for which electrons can only heat the background medium and photons which can ionize the neutral atoms, we can compute the electromagnetic cascade and energy deposition fraction of higher energy injected particles. The calculation thus proceeds in a recursive way, from low energy to high energies. More details can be found in [52].

### 3 Time evolution of evaporating black holes

We consider Schwarzschild black holes in this work. Since for a rotating black hole, more than 50 percent of the black hole energy is emitted when the black hole has already lost most of its spin [63], this is a good approximation. The spectrum of the emitted particles just outside the horizon of the black hole is given by a thermal distribution with Hawking temperature (with  $c = \hbar = k_B = 1$ , where  $c$  is the speed of light,  $\hbar = \frac{h}{2\pi}$ ,  $h$  is the Planck constant,  $k_B$  is the Boltzmann constant) [8, 43],

$$T_{\text{BH}} = \frac{1}{8\pi G M_{\text{BH}}} = 1.06 M_{10}^{-1} \text{ TeV}, \quad (3.1)$$

where  $M_{10} = M_{\text{BH}}/10^{10} \text{ g}$  is the instantaneous mass of black hole in units of  $10^{10} \text{ g}$ . Since, the emitted particles initially propagate in the gravitational potential well of the black hole, the actual spectrum of emitted particles, far from the black hole, deviates from a pure thermal spectrum and this deviation is captured by the absorption coefficient  $\Gamma_s(E, M_{\text{BH}}, m)$  [64, 65], where  $s$  is the spin of the emitted particle,  $E$  is the energy of the emitted particle,  $M_{\text{BH}}$  is the mass of the black hole, and  $m$  is the mass of the emitted particle. The effective potential as seen by a propagating particle outside the black hole is a function of black hole mass, particle mass and particle spin [66]. With this correction, the emitted spectrum of black hole in the

energy interval  $E$  and  $E + dE$  is given by,

$$\frac{dN}{dt} = \frac{\Gamma_s(E, M_{\text{BH}}, m)}{2\pi} \frac{1}{e^{E/T_{\text{BH}}} - (-1)^{2s}} dE. \quad (3.2)$$

At high energy ( $E \gg T_{\text{BH}}$ ), the absorption coefficients become independent of particle mass and spin and approach the thermal limit  $\Gamma_s(E/T_{\text{BH}} \gg 1) = 27G^2M^2$ . The evaporation of the black holes changes their temperature which in turn changes the spectrum of the emitted particles. Therefore, for accurate calculation of energy cascades from black hole evaporation, we have to keep track of the black hole temperature or mass as it evaporates. The mass loss rate from evaporating black holes can be written as [67],

$$\frac{dM_{\text{BH}}}{dt} = -5.34 \times 10^{25} \frac{f(M_{\text{BH}})}{M_{\text{BH}}^2} \text{gs}^{-1}. \quad (3.3)$$

where  $f(M_{\text{BH}})$  is approximately given by,

$$\begin{aligned} f(M_{\text{BH}}) = & 1.0 + 0.569 \left[ \exp\left(-\frac{M_{\text{BH}}}{x_{\text{bh},s=1/2} M_e^T}\right) + \exp\left(-\frac{M_{\text{BH}}}{x_{\text{bh},s=1/2} M_\mu^T}\right) + 3 \exp\left(-\frac{M_{\text{BH}}}{x_{\text{bh},s=1/2} M_u^T}\right) \right] Q_{\text{QCD}} \\ & + 3 \exp\left(-\frac{M_{\text{BH}}}{x_{\text{bh},s=1/2} M_d^T}\right) Q_{\text{QCD}} + 3 \exp\left(-\frac{M_{\text{BH}}}{x_{\text{bh},s=1/2} M_s^T}\right) Q_{\text{QCD}} + 3 \exp\left(-\frac{M_{\text{BH}}}{x_{\text{bh},s=1/2} M_c^T}\right) Q_{\text{QCD}} \\ & + \exp\left(-\frac{M_{\text{BH}}}{x_{\text{bh},s=1/2} M_\tau^T}\right) Q_{\text{QCD}} + 3 \exp\left(-\frac{M_{\text{BH}}}{x_{\text{bh},s=1/2} M_b^T}\right) Q_{\text{QCD}} \\ & + 0.963 \exp\left(-\frac{M_{\text{BH}}}{x_{\text{bh},s=1} M_g^T}\right) Q_{\text{QCD}} + 0.267 \exp\left(-\frac{M_{\text{BH}}}{x_{\text{bh},s=0} M_{\pi^0}^T}\right) (1 - Q_{\text{QCD}}) \\ & + 2.0 \times 0.267 \left[ \exp\left(-\frac{M_{\text{BH}}}{x_{\text{bh},s=0} M_{\pi^+}^T}\right) (1 - Q_{\text{QCD}}) \right], \quad (3.4) \end{aligned}$$

with

$$M_i^T = \frac{1}{8\pi G m_i}, \quad (3.5)$$

where  $M_i^T$  is the mass of the black hole whose temperature is equal to the mass  $m_i$  of the standard model particle, where  $i \in (e, \mu, \pi^0, \pi^+, u, d, s, c, \tau, b, g)$  for electron, muon, neutral and charged pions, up quark, down quark, strange quark, charm quark, tau, bottom quark and gluon respectively,  $x_{\text{bh}} = \frac{E}{T_{\text{BH}}}$ , and  $x_{\text{bh},s}$  is the location of the peak of the emitted instantaneous power spectrum,  $\frac{\gamma_s(x_{\text{bh}}) x_{\text{BH}}^3}{e^{x_{\text{bh}}} - (-1)^{2s}}$  with  $\gamma_s(x_{\text{bh}}) = \Gamma_s(E)/27G^2M^2$ . The value of  $x_{\text{bh},s}$  for  $s=0, 1/2$ , and 1 is 2.66, 4.53, and 6.04 respectively [67]. We use the updated list of mass of particles from [68]. The effect of QCD phase transition is captured in  $Q_{\text{QCD}}$  with  $Q_{\text{QCD}} = [1 + \exp(\frac{-\log_{10}(T_{\text{BH}}/T_{\text{QCD}})}{\sigma})]$  [47, 50],  $T_{\text{QCD}}=300$  MeV, and  $\sigma=0.1$ . We assume that above 300 MeV, the kinematical mass of up and down quarks [69, 70], quarks are freely emitted and below this energy only pions are produced as shown in Fig. 1b. For the black holes with mass  $M_{\text{BH}} \gtrsim 10^{13}$ g, the contribution of W and Z bosons, higgs and top quark is negligible (Fig. 1a) and therefore, is neglected. Freely emitted quarks, gluons, pions, muons and tau will

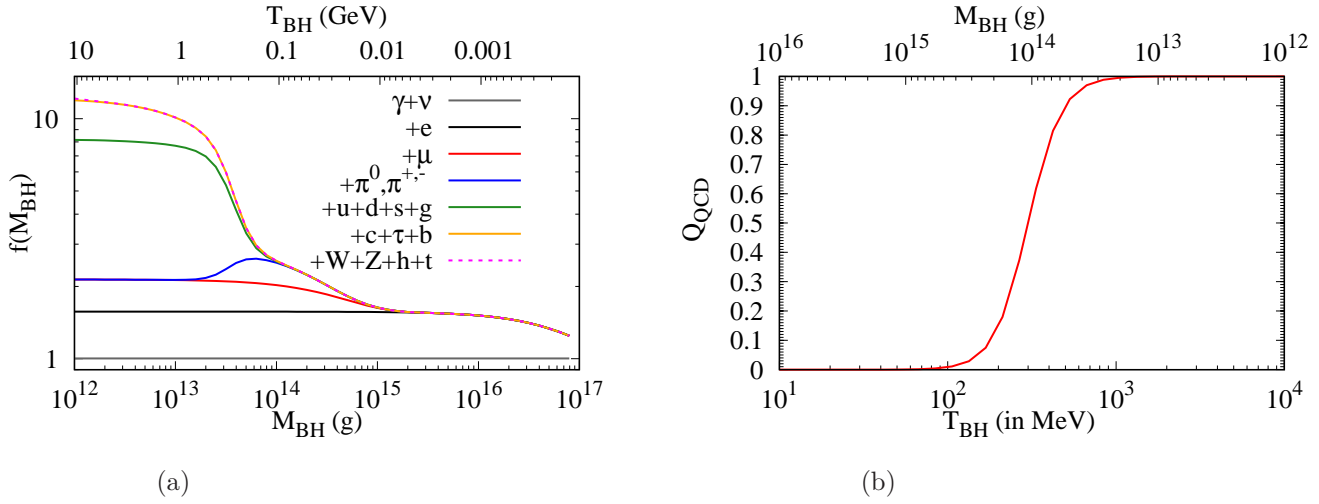


**Figure 1:** The parameters (a)  $f(M_{\text{BH}})$ , (b)  $Q_{\text{QCD}}(T_{\text{BH}})$  defined in Eq. 3.4 as a function of black hole mass and temperature.

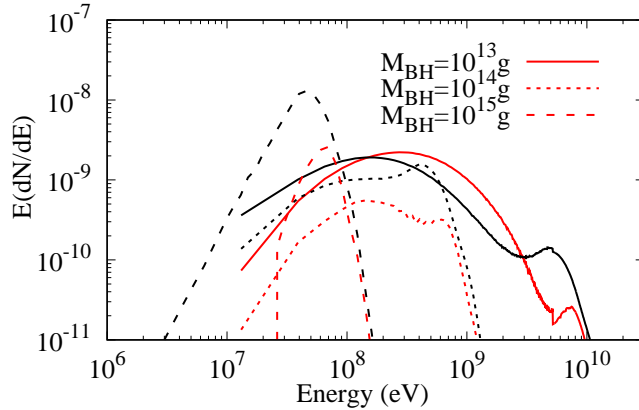


**Figure 2:** Instantaneous spectrum of electron-positron pairs (black) and photons (red) at redshift  $z = 10000$  for different black hole mass. We have plotted the number of particles per unit log energy ( $E dN/dE$ ).

hadronize or decay to produce secondary photons, electrons and positrons. To calculate the secondary photon, electron and positron spectrum, we have used PYTHIA 8.2 [69, 70]. We use the script available with PYTHIA 8.2 for hadronization of quarks and gluons and decay of taus, muons and any unstable hadrons produced during hadronization. The output obtained for a monochromatic particle (i.e. quark or muon injection etc.) is tabulated as spectra of stable standard model particles i.e. electrons, positrons, photons, neutrinos and stable hadrons (proton and deuterium). Any injection spectrum which is non-monochromatic can be thought of as a superposition of monochromatic energy injection and the tabulated results

for monochromatic energies is used to obtain the final particle spectrum. In Fig. 2, we plot the instantaneous spectra of emitted electron-positron pairs and photons at  $z=10000$ , when the black holes are almost intact. The temperature of black hole with mass  $10^{13}\text{g}$  is  $\sim 1$  GeV. The quarks and gluons produce secondary photons and electron-positron pairs which dominate the output spectrum. The peaks at high energy end is due to primary emission of photons and electron-positron pairs. For black hole mass  $\gtrsim 10^{14}\text{g}$ , primary emission of photons, electrons and positrons dominate the output spectrum as quark, gluon, pion, and muon channels shut down.

#### 4 Energy deposition from black hole evaporation

Energy injection rate from evaporating black holes is given by,

$$\frac{dE_{\text{inj}}}{dt} = f_{\text{BH}}\rho_c c^2(1+z)^3 \frac{dM_{\text{BH}}/dt}{M_{\text{BH},0}}, \quad (4.1)$$

where  $f_{\text{BH}} = \frac{\rho_{\text{BH}}}{\rho_c}$  is the fraction PBH energy density ( $\rho_{\text{BH}}$ ) w.r.t to the stable cold dark matter energy density ( $\rho_c$ ),  $M_{\text{BH},0}$  is the mass of the black hole before evaporation. The energy injected in a time interval  $\Delta t$  (in a redshift step  $\Delta z$ ) is given by,  $\Delta E_{\text{inj}} = \frac{dE_{\text{inj}}}{dt} \Delta t$ , where  $\Delta t = \frac{|\Delta z|}{(1+z)H(z)}$ , and  $H(z)$  is the Hubble rate. The deposited energy fraction at a redshift  $z$  is defined as,

$$f_{\text{dep}}(z) = \frac{\Delta E_{\text{dep}}/\Delta t}{\Delta E_{\text{inj}}/\Delta t}, \quad (4.2)$$

where  $\Delta E_{\text{dep}}$  is the energy deposited during redshift interval between  $z$  and  $z - \Delta z$ . The fraction of energy going into ionization of neutral hydrogen is defined as,

$$f_{\text{H,ion}}(z) = \frac{\Delta E_{\text{H,ion}}/\Delta t}{\Delta E_{\text{inj}}/\Delta t}, \quad (4.3)$$

where  $\Delta E_{\text{H,ion}} \equiv \Delta N_{\text{H,ion}} \times 13.6 \text{ eV}$  and  $\Delta N_{\text{H,ion}}$  is the number of ionizations from energy injection.

The energy injected by PBH is deposited in the background baryonic gas as heating, excitation of neutral hydrogen and helium, and ionization of neutral hydrogen, neutral helium, and singly ionized helium. Low energy photons with energy less than the Lyman-alpha threshold of hydrogen are not deposited to the baryonic gas and they have a completely negligible effect on the recombination process. However, we still tag them as deposited energy for the purpose of accounting. These photons must be followed separately if we want to calculate their contribution to the CMB spectral distortions. Energy deposited at a particular redshift includes contribution from energy injection at that redshift and earlier redshifts. In Fig. 3, we plot the fraction of evaporating black holes' energy going into hydrogen ionization as a function of redshift for different values of PBH mass. To calculate the energy deposition fractions, standard recombination history [16, 17] is assumed for all cases. This is a good approximation since the modification to the recombination history due to energy injection is

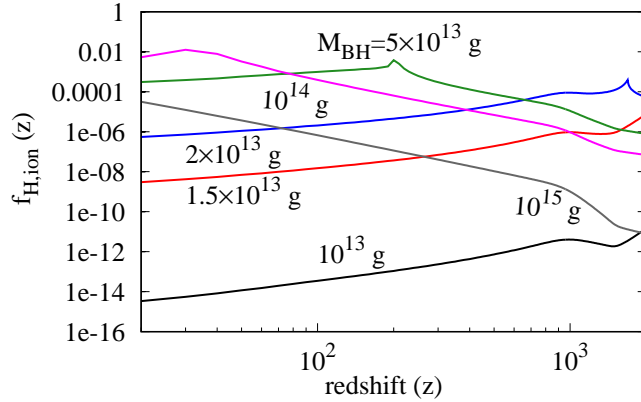


**Figure 3:** Fraction of injected energy going to hydrogen ionization as a function of redshift for PBHs of different masses.

small, and therefore does not change the energy deposition fraction significantly. We have used the **Recfast++** module [71, 72] of **CosmoRec** code [72–79] to solve for the recombination history with energy injection due to PBHs. We have neglected excitations as they do not make a significant difference [52]. A detailed discussion on the effect of the choice of recombination code on the CMB anisotropy power spectrum can be found in [52].

For the black holes evaporating before the recombination epoch ( $M_{\text{BH},0} \lesssim 10^{13}$  g), a fraction of energy survives and is not deposited until after the recombination epoch, and thus can affect the CMB anisotropy power spectrum. The black holes with mass  $M_{\text{BH},0} > 10^{14}$  g are mostly intact until reionization. The cuspy feature around redshift 200 in Fig. 3 corresponds approximately to the redshift at which the black hole with mass  $5 \times 10^{13}$  g completely evaporates and thus injects most of its mass-energy into the plasma i.e. the redshift corresponding to the lifetime of the black hole. As can be seen from Eq. 3.3, the rate of evaporation of black hole increases as the black hole gradually evaporates. Therefore, most of the black hole’s energy is evaporated in a small redshift range [80]. This substantially increases the energy deposition at the redshift where most of the black hole evaporates giving rise to an increase in the energy deposition fraction. Once the black hole has evaporated away, there is no more energy injection and the deposited energy from energy injected at earlier times gradually decreases with time. For black hole with mass heavier than  $5 \times 10^{13}$  g, the black holes are still intact. Since, there is tiny amount of energy injection from black holes, the fraction of energy deposited with respect to the unevaporated black hole mass is small. The deposition fraction of these heavier black holes increases with decreasing redshifts as black hole evaporation proceeds. For mass smaller than  $5 \times 10^{13}$  g, lesser and lesser energy are deposited with decreasing redshifts as most of the energy has been deposited at higher redshifts.

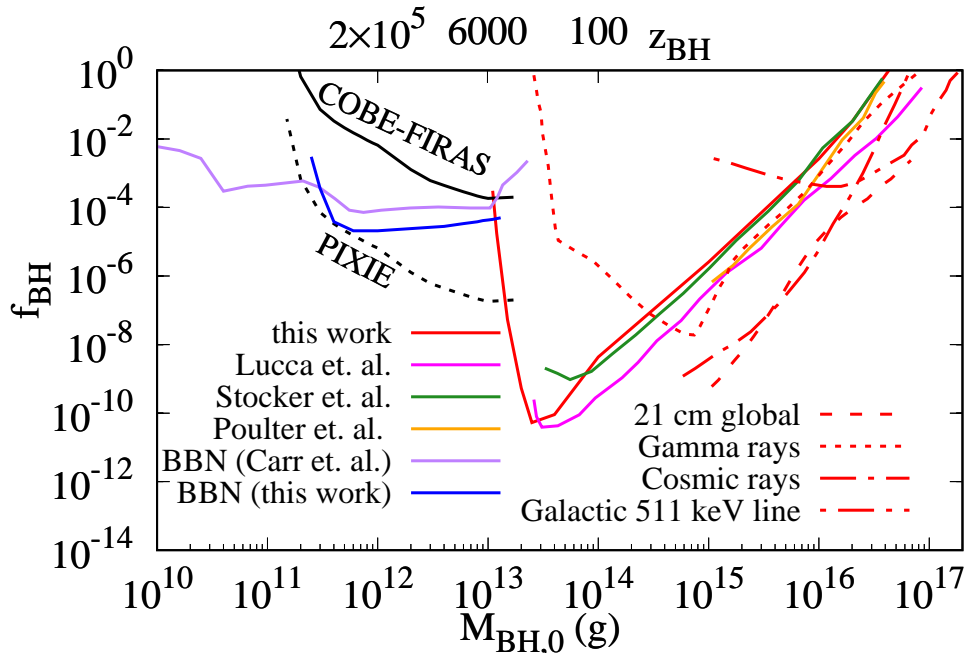


**Figure 4:**  $2\text{-}\sigma$  constraints (upper limits) on the abundance of PBHs as a function of mass derived in this work using CMB anisotropies and abundance of light elements. The evaporation redshift ( $z_{\text{BH}}$ ) corresponds to the redshift at which the mass of the black hole of a given mass reduces by a factor of  $e(=2.718)$ . Comparison with previous works of Stocker et. al. [47], Poulter et. al. [51], and Lucca et. al. [50] is shown. We also show spectral distortion constraints using COBE-FIRAS data [81, 82] derived in [80] as well as projection from a future PIXIE-like experiment assuming a factor of 1000 improvement over COBE-FIRAS. We also show BBN constraints from Fig. 9 of [50] which were adapted from [8, 53], constraints from global 21 cm signal [54], gamma rays (taken from [56], non-spinning case), cosmic rays [57] (model A with background), and 511 keV gamma ray line from galactic center (taken from [60]) for comparison.

## 5 Planck CMB anisotropy, BBN and CMB spectral distortions constraints on PBHs

We show the main results of this paper in Fig. 4. We do a Markov chain Monte carlo (MCMC) analysis with the publicly available code **COSMOMC** [84] and use **Recfast++** module of **CosmoRec** [72] to solve for the recombination history. We fit for  $f_{\text{BH}}$  along with the 6 standard cosmological parameters [48] using Planck2018 PlikTT,TE,EE and low E likelihood [85]. We assume monochromatic mass function and perform the fit for different initial black hole mass  $M_{\text{BH},0}$  and obtain constraints on  $f_{\text{BH}}$  as a function of  $M_{\text{BH},0}$ . We show  $2\text{-}\sigma$  upper limits in Fig. 4. For abundance of light elements from BBN, we find that the abundance of helium-3 ( ${}^3\text{He}$ ) gives the strongest constraints. The initial abundance of

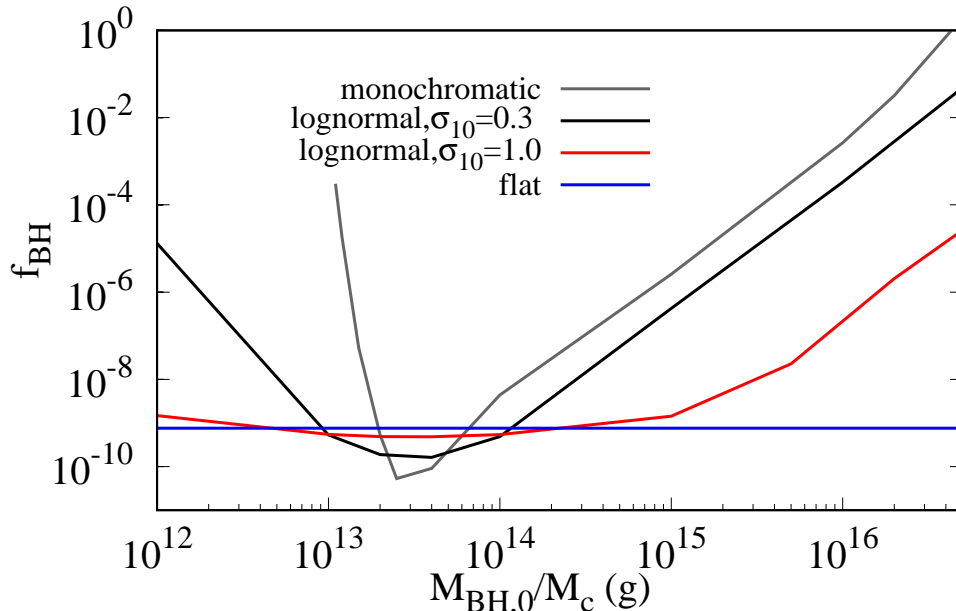


**Figure 5:** Constraints on black holes with extended mass distribution. We consider lognormal distribution with two different variances and a flat distribution with lower and upper limits for mass being  $10^{12}$ g and  $5 \times 10^{16}$ g respectively. The x-axis denotes  $M_{\text{BH},0}$  for monochromatic and  $M_c$  for lognormal mass distribution in Eq. 5.1.

${}^3\text{He}$  before black hole evaporation is taken to be the theoretical  $2\text{-}\sigma$  lower limit prediction from BBN for Planck cosmological parameters. Constraints are obtained by allowing the maximum abundance, after creating extra  ${}^3\text{He}$  from  ${}^4\text{He}$  photo-dissociation, to be at the  $2\text{-}\sigma$  observed upper limit. We also show the CMB spectral distortion constraints obtained in [80] from Cosmic Background Explorer-Far Infrared Absolute Spectrophotometer (COBE-FIRAS) data and projections for the Primordial Inflation Explorer (PIXIE) or similar mission assuming a factor of 1000 improvement over COBE-FIRAS.

Our results show that the Planck CMB anisotropy measurements put stronger constraints compared to the BBN and CMB spectral distortions from COBE-FIRAS [81] on the abundance of primordial black holes with mass  $M_{\text{BH},0} \geq 1.1 \times 10^{13}$ g. This limit is slightly lower compared to the mass of  $3 \times 10^{13}$ g upto which CMB anisotropy constraints were calculated in [47, 50]. A fraction of high energy photons injected before the recombination epoch can survive until the end of the recombination epoch and deposit their energy once the universe becomes neutral. The much high precision with which the CMB anisotropies are measured and the sensitivity of the CMB anisotropy power spectrum to small changes in the recombination history means that the CMB anisotropy power spectrum can provide competitive CMB anisotropy constraints compared to BBN and spectral distortions even for

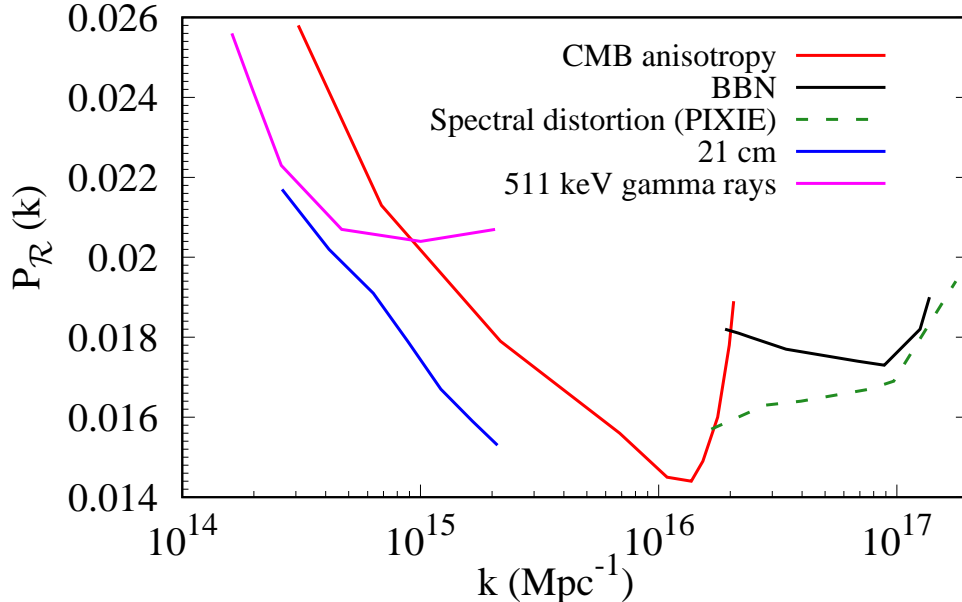


**Figure 6:** Constraints on primordial curvature power spectrum as a function of comoving wave number from CMB anisotropies, BBN calculations in this work and PIXIE [83] projection from [80]. Also shown are 21 cm and 511 keV gamma rays constraints from Fig. 4, which are the strongest constraints in the mass range  $10^{15}\text{g} - 10^{17}\text{g}$ .

pre-recombination energy injection. Our results agree with the results of Lucca et. al. [50] for black holes evaporating at  $z \sim 1000$ . Lucca et. al. use on-the-spot approximation for energy deposition which is a reasonable approximation for energy injections at  $z \sim 1000$  but this approximation will over-estimate the deposition efficiency at lower redshifts. Therefore, we expect our constraints without on-the-spot approximation to be weaker for black holes evaporating at redshifts  $z < 1000$ . Our results agree with the result of Stocker et. al. [47] for black holes with initial temperatures less than the QCD phase transition. The authors in [47] use the results of Slatyer et. al. [49] to calculate the energy deposition fractions. However, there may be possible numerical errors in taking into account QCD phase transition in [47] (see discussions in [50]). This might explain the difference between our results and [47] for PBH mass smaller than  $10^{14}\text{g}$ , precisely at the point when the black hole temperature is of the order  $\sim 100$  MeV. We have reasonable agreement with the results of Poulter et. al. [51] who also use the results of [49] without on-the-spot approximation. For the mass range considered in [51], temperature of black hole is below the QCD phase transition. However, the authors have made approximations such as considering the universe to be completely matter dominated below  $z < 3000$  which would have affected their quantitative results.

We also show our BBN constraints with full evolution of electromagnetic cascades

in an expanding universe. For comparison, we also plot BBN constraints from Fig. 9 of [50] which is adapted from [8, 53]. The BBN constraints in [8, 53] are derived taking into account both electromagnetic and hadronic interactions of emitted particles (electrons, positrons, photons, nucleons and antinucleons) with background electrons, photons and hadrons. Since we ignore the hadronic interactions with primordial nuclei which would also result in their destruction, our results would be expected to be slightly weaker or conservative compared to [8, 53]. Nevertheless, we would like to point out that with the current constraints on  ${}^3\text{He}$ , significantly stronger constraints than the constraints in [8] are possible. The authors in [8] consider 2- $\sigma$  upper bound on ratio of deuterium  ${}^2\text{H}$  to hydrogen (H) abundance to be,  $\frac{n_{{}^2\text{H}}}{n_{\text{H}}} = 5.16 \times 10^{-5}$  and for ratio of  ${}^3\text{He}$  to deuterium to be  $\frac{n_{{}^3\text{He}}}{n_{{}^2\text{H}}} = 1.37$ , where  $n_{{}^3\text{He}}$ ,  $n_{{}^2\text{H}}$  and  $n_{\text{H}}$  are the observed helium-3, deuterium and hydrogen number density respectively. Our 2- $\sigma$  upper limit on  ${}^3\text{He}$  abundance is  $\frac{{}^3\text{He}}{\text{H}} = 1.5 \times 10^{-5}$  [86]. With the new upper limits from observations but neglecting energy going into stable nucleons, we conservatively get BBN constraints which are stronger than the constraints in [8] by upto a factor of 4-5. The BBN constraints in [8] for black hole mass below  $\lesssim 4 \times 10^{11}\text{g}$  are due to lithium which we do not consider in this work.

We also show the CMB spectral distortion constraints from COBE-FIRAS [81] derived in [80] and projections for PIXIE [83] assuming a factor of 1000 improvement over COBE-FIRAS. The spectral distortion constraints are derived with full electromagnetic cascade evolution which can be substantially different from thermal ( $y$ ,  $i$  or  $\mu$ ) distortions due to contributions from non-thermal relativistic particles. For primordial black holes with mass  $\approx 10^{13}\text{g}$ , the actual constraints, taking into account the actual shape of non-thermal distortions, are relaxed by a factor of 2 compared to the constraints using the yim approximation.

We also show, for comparison, the constraints from 21 cm line observations, gamma rays, cosmic rays, and 511 keV galactic gamma rays in Fig. 4. Energy injection from primordial black hole evaporation can heat and ionize the intergalactic medium and modify the global 21 cm spin temperature evolution. Requiring that the 21 cm absorption signal during the reionization epoch does not get wiped out from electromagnetic energy injection, we can put constraints on evaporating black holes [54]. However, these constraints have to be re-derived considering EDGES [87] result which require new physics or consideration of astrophysical uncertainties. Primordial black holes evaporating today ( $M_{\text{BH},0} \sim 10^{15}\text{g}$ ) emit photons and electron-positron pairs dominantly. Using the diffuse gamma ray background [56], cosmic ray  $e^-e^+$  [57] and 511 keV gamma rays from annihilation of  $e^-e^+$  at galactic center [60], we can put constraints on abundance of evaporating black holes in the mass range  $M_{\text{BH},0} \gtrsim 10^{15}\text{g}$ .

In Fig. 5, we show the constraints on black holes with extended mass functions. We use the prescription of [10] to convert monochromatic mass constraints to extended mass constraints. We consider lognormal distribution with mass function,

$$\psi(M_{\text{BH},0}) = \frac{f_{\text{BH}}}{\sqrt{2\pi}\sigma M_{\text{BH},0}} \exp\left(-\frac{(\ln(M_{\text{BH},0}/M_c))^2}{2\sigma^2}\right), \quad (5.1)$$

where  $M_c$  is the center of mass distribution and  $\sigma$  is the variance. We can convert the base in the log from e to 10 to suit our numbers [51]. In that case  $\sigma = \sigma_{10}\ln(10)$ . The constraints for extended mass spectrum with center  $M_c$  are in general stronger compared to monochromatic spectrum due to contribution of stronger constraints from monochromatic mass with  $M_{\text{BH},0}$  different from  $M_c$ . In the opposite case, when the monochromatic constraints with  $M_{\text{BH},0} = M_c$  are the strongest, the presence of other black holes with different mass in the extended mass function make the constraints for extended mass function weaker. The black holes with different masses have different energy injection histories and the effect of black hole evaporation on the CMB for different masses will not be strictly additive. These constraints are therefore only approximate but sufficient to give a qualitative idea about what to expect for extended mass functions.

## 6 Constraints on primordial power spectrum and 40 e-folds of inflation

Since PBH are formed from fluctuations of density perturbations in the early Universe, we can put constraints on the initial power spectrum from the allowed abundance of PBH [11, 88–92]. In Fig. 6, we show constraints on primordial curvature power spectrum  $P_R(k)$  as a function of comoving wave number ( $k$ ) from CMB anisotropies and BBN calculations, done in this work, as well as PIXIE forecasts which can be in principle be stronger compared to the current BBN constraints. We also show 21 cm and 511 keV gamma rays constraints, which are the strongest constraints in the low  $k$  part of parameter space. We follow the procedure of [92] to translate the constraints on  $f_{\text{BH}}$  to the constraints on  $P_R(k)$ . Mass of PBH formed in a particular epoch is given by,

$$M_{\text{BH},0} = \frac{4\pi}{3}\gamma\rho H^{-3}, \quad (6.1)$$

where  $\gamma = 0.2$  [8, 11],  $\rho$  is the average total energy density of the Universe and  $1/H$  is the horizon size at that epoch. In Press-Schechter theory, PBH form if the smoothed density perturbation is above a certain threshold  $\delta_c$ , which was derived to be 0.42 in a radiation dominated universe in [93, 94]. The density field on smoothing scale  $R$ ,  $\delta(R)$ , is assumed to have a gaussian distribution,

$$P(\delta(R)) = \frac{1}{\sqrt{(2\pi)\sigma(R)}} \exp\left(-\frac{\delta^2(R)}{2\sigma^2(R)}\right), \quad (6.2)$$

where  $\sigma^2(R) = \int_0^\infty W^2(kR)P_\delta(k)\frac{dk}{k}$ ,  $R = 1/(aH)$ ,  $a$  is the scale factor,  $W(kR)$  is a window function to smoothen the density perturbations which we assume to be Gaussian. The relative abundance of PBH is obtained by integral of the probability distribution of density perturbation with density fluctuations greater than  $\delta_c$ , i.e.

$$\beta = 2 \int_{\delta_c}^1 d\delta(R)P(\delta(R)) \approx \text{erfc}\left(\frac{\delta_c}{\sqrt{2}\sigma(R)}\right). \quad (6.3)$$

We can obtain  $\beta$  from  $f_{\text{BH}}$  by using the relation [92],

$$\beta(M_{\text{BH},0}) = 4.0 \times 10^{-9} \left( \frac{g_*^i}{10.75} \right)^{1/4} \left( \frac{M_{\text{BH},0}}{2 \times 10^{33} \text{g}} \right)^{1/2} f_{\text{BH}}, \quad (6.4)$$

where  $g_*^i$  is the total radiative degrees of freedom at the formation epoch of PBH. The average energy of the standard model particles or the temperature of the Universe at the formation epoch of black holes considered in this work is in the range of  $10^{17} \text{eV}$ - $10^{20} \text{eV}$ . Since, this energy scale is much higher than the mass scale of all standard model particles, we take  $g_*^i$  to be 106 using the standard model of particle physics. The relation to convert density perturbation to curvature perturbation is given by [95],

$$\delta(k, t) = \frac{2(1+3w)}{(5+3w)} (k/aH)^2 \mathcal{R}, \quad (6.5)$$

with  $w = 1/3$ , where  $w$  is the equation of state in the radiation dominated era. Power spectrum of density fluctuations can then be related to power spectrum of curvature perturbation as,

$$P_\delta(k, t) = \left( \frac{2(1+3w)}{(5+3w)} \right)^2 (k/aH)^4 P_{\mathcal{R}}(k), \quad (6.6)$$

We assume slow-roll like inflationary power spectrum  $P_{\mathcal{R}}(k) = P_{\mathcal{R}}(k_0) \left( \frac{k}{k_0} \right)^{n_s - 1}$  with  $n_s \sim 1$ . Obtaining  $\sigma(R)$  from Eq. 6.3 and substituting Eq. 6.6 in the expression of  $\sigma(R)$ , we calculate  $P_{\mathcal{R}}(k_0)$  for a given  $f_{\text{BH}}(M_{\text{BH},0})$  with  $k_0 = aH$ , where  $a$  and  $H$  are the scale factor and Hubble parameter at the time of black hole formation related to  $M_{\text{BH},0}$  by Eq. 6.1. In Fig. 6, we provide constraints on amplitude of the primordial power spectrum from constraints on abundance of PBH obtained in this work as well as 21 cm and 511 keV galactic gamma rays constraints which are stronger in appropriate mass range. Together, these probes put an upper bound on the amplitude of the primordial power spectrum on the scales of  $10^{14} \text{Mpc}^{-1} \lesssim k \lesssim 10^{17} \text{Mpc}^{-1}$ . The perturbations on these scales were created towards the end of inflation, about  $\sim 40$  e-folds after the modes observed in the CMB anisotropies and large scale structure went out of horizon during inflation. Therefore, combined with the CMB anisotropies, PBH provide a view of almost the entire inflationary history. In particular, the abundance of PBH are almost the only observational constraints on this epoch of inflation just before inflation ends. Constraints on the abundance of the PBH in the mass range  $10^{11} \text{g}$ - $10^{17} \text{g}$  nicely complement the constraints from heavier black holes ( $k \lesssim 10^{14} \text{Mpc}^{-1}$  [92]) and CMB spectral distortions constraints from acoustic damping on the scales of  $k \lesssim 10^4 \text{Mpc}^{-1}$  [96].

## 7 Conclusions

In this work, we provide CMB anisotropy power spectrum constraints and BBN constraints on evaporating black holes with our own calculations of the evolution of the electromagnetic

particle cascade in an expanding universe. Our constraints are based on the precise treatment of electromagnetic cascades in a consistent framework for all three data sets relevant during and before recombination, namely, CMB anisotropies, spectral distortions, and BBN abundances of elements. We have shown that the CMB anisotropies can constrain black holes with slightly lower mass compared to the previous calculations. We obtain good agreement with previous literature in the regime where the approximations used in those calculations are reasonable. We also provide BBN constraints with more up-to-date observational values of helium-3 abundance. Even with a factor of 1000 improvement in future with PIXIE-like mission, CMB anisotropies will still provide stronger constraints for  $M_{\text{BH},0} \geq 10^{13}\text{g}$ . Our work, in particular, fills the small gap that existed between the BBN/spectral distortions constraints and CMB anisotropy constraints. Even though the black holes considered in this paper would have been completely evaporated by now, the limits on their existence in the early universe provide important constraints on perturbations generated during the last stages of inflation corresponding to the modes on scales  $10^{14} \text{ Mpc}^{-1} \lesssim k \lesssim 10^{17} \text{ Mpc}^{-1}$ ,  $\sim 40$  e-folds after the modes we observe in the CMB anisotropies and large scale structure of the Universe went out of horizon during inflation.

## 8 Acknowledgements

We acknowledge the use of computational facilities of Department of Theoretical Physics at Tata Institute of Fundamental Research, Mumbai. This work was supported by Max Planck Partner Group for cosmology of Max Planck Institute for Astrophysics Garching at Tata Institute of Fundamental Research funded by Max-Planck-Gesellschaft. This work was also supported by Science and Engineering Research Board (SERB) of Department of Science and Technology, Government of India grant no. ECR/2015/000078. We acknowledge support of the Department of Atomic Energy, Government of India, under project no. 12-R&D-TFR-5.02-0200.

## References

- [1] Simeon Bird, Ilias Cholis, Julian B. Muñoz, Yacine Ali-Haïmoud, Marc Kamionkowski, Ely D. Kovetz, Alvise Raccanelli, and Adam G. Riess. Did LIGO Detect Dark Matter? *Phys.Rev.Lett*, 116(20):201301, May 2016. [arXiv:1603.00464](#), [\[DOI\]](#), [\[ADS\]](#).
- [2] LIGO Scientific Collaboration Abbott, B. P. et. al. and Virgo Collaboration. Observation of Gravitational Waves from a Binary Black Hole Merger. *Phys.Rev.Lett*, 116(6):061102, Feb 2016. [arXiv:1602.03837](#), [\[DOI\]](#), [\[ADS\]](#).
- [3] Bernard Carr, Florian Kühnel, and Marit Sandstad. Primordial black holes as dark matter. *Phys.Rev.D*, 94(8):083504, Oct 2016. [arXiv:1607.06077](#), [\[DOI\]](#), [\[ADS\]](#).
- [4] Y. B. Zel’dovich and I. D. Novikov. The Hypothesis of Cores Retarded during Expansion and the Hot Cosmological Model. *Astronomicheskii Zhurnal*, 43:758, 1966. [\[ADS\]](#).
- [5] S. Hawking. Gravitationally collapsed objects of very low mass. *MNRAS*, 152:75, 1971. [\[DOI\]](#), [\[ADS\]](#).

- [6] B. J. Carr and S. W. Hawking. Black holes in the early Universe. *MNRAS*, 168:399–416, August 1974. [\[DOI\]](#), [\[ADS\]](#).
- [7] I. D. Novikov, A. G. Polnarev, A. A. Starobinskii, and Ia. B. Zeldovich. Primordial black holes. *A&A*, 80(1):104–109, November 1979. [\[ADS\]](#).
- [8] B. J. Carr, Kazunori Kohri, Yuuiti Sendouda, and Jun’ichi Yokoyama. New cosmological constraints on primordial black holes. *Phys.Rev.D*, 81:104019, May 2010. [arXiv:0912.5297](#), [\[DOI\]](#), [\[ADS\]](#).
- [9] Florian Kühnel and Katherine Freese. Constraints on primordial black holes with extended mass functions. *Phys.Rev.D*, 95(8):083508, Apr 2017. [arXiv:1701.07223](#), [\[DOI\]](#), [\[ADS\]](#).
- [10] Bernard Carr, Martti Raidal, Tommi Tenkanen, Ville Vaskonen, and Hardi Veermäe. Primordial black hole constraints for extended mass functions. *Phys.Rev.D*, 96(2):023514, Jul 2017. [arXiv:1705.05567](#), [\[DOI\]](#), [\[ADS\]](#).
- [11] B. J. Carr. The primordial black hole mass spectrum. *ApJ*, 201:1–19, Oct 1975. [\[DOI\]](#), [\[ADS\]](#).
- [12] Raziieh Emami and George F. Smoot. Observational constraints on the primordial curvature power spectrum. *JCAP*, 2018(1):007, Jan 2018. [arXiv:1705.09924](#), [\[DOI\]](#), [\[ADS\]](#).
- [13] Massimo Ricotti, Jeremiah P. Ostriker, and Katherine J. Mack. Effect of Primordial Black Holes on the Cosmic Microwave Background and Cosmological Parameter Estimates. *ApJ*, 680:829–845, Jun 2008. [arXiv:0709.0524](#), [\[DOI\]](#), [\[ADS\]](#).
- [14] Y. Ali-Haïmoud and M. Kamionkowski. Cosmic microwave background limits on accreting primordial black holes. *Phys.Rev.D*, 95(4):043534, February 2017. [arXiv:1612.05644](#), [\[DOI\]](#), [\[ADS\]](#).
- [15] Vivian Poulin, Pasquale D. Serpico, Francesca Calore, Sébastien Clesse, and Kazunori Kohri. CMB bounds on disk-accreting massive primordial black holes. *Phys.Rev.D*, 96(8):083524, Oct 2017. [arXiv:1707.04206](#), [\[DOI\]](#), [\[ADS\]](#).
- [16] Y. B. Zel’dovich, V. G. Kurt, and R. A. Syunyaev. Recombination of Hydrogen in the Hot Model of the Universe. *Soviet Journal of Experimental and Theoretical Physics*, 28:146, January 1969. [\[ADS\]](#).
- [17] P. J. E. Peebles. Recombination of the Primeval Plasma. *ApJ*, 153:1, July 1968. [\[DOI\]](#), [\[ADS\]](#).
- [18] J. A. Adams, S. Sarkar, and D. W. Sciama. Cosmic microwave background anisotropy in the decaying neutrino cosmology. *MNRAS*, 301:210–214, November 1998. [arXiv:astro-ph/9805108](#), [\[DOI\]](#), [\[ADS\]](#).
- [19] X. Chen and M. Kamionkowski. Particle decays during the cosmic dark ages. *Phys.Rev.D*, 70(4):043502, August 2004. [arXiv:astro-ph/0310473](#), [\[DOI\]](#), [\[ADS\]](#).
- [20] N. Padmanabhan and D. P. Finkbeiner. Detecting dark matter annihilation with CMB polarization: Signatures and experimental prospects. *Phys.Rev.D*, 72(2):023508, July 2005. [arXiv:astro-ph/0503486](#), [\[DOI\]](#), [\[ADS\]](#).
- [21] T. R. Slatyer, N. Padmanabhan, and D. P. Finkbeiner. CMB constraints on WIMP annihilation: Energy absorption during the recombination epoch. *Phys.Rev.D*, 80(4):043526, August 2009. [arXiv:0906.1197](#), [\[DOI\]](#), [\[ADS\]](#).

- [22] S. Galli, F. Iocco, G. Bertone, and A. Melchiorri. CMB constraints on dark matter models with large annihilation cross section. *Phys.Rev.D*, 80(2):023505, July 2009. [arXiv:0905.0003](#), [\[DOI\]](#), [\[ADS\]](#).
- [23] Y. B. Zeldovich and R. A. Sunyaev. The Interaction of Matter and Radiation in a Hot-Model Universe. *ApSS*, 4:301–316, July 1969. [\[DOI\]](#), [\[ADS\]](#).
- [24] R. A. Sunyaev and Y. B. Zeldovich. The interaction of matter and radiation in the hot model of the Universe, II. *ApSS*, 7:20–30, April 1970. [\[DOI\]](#), [\[ADS\]](#).
- [25] A. F. Illarionov and R. A. Siuniaev. Comptonization, the background-radiation spectrum, and the thermal history of the universe. *Soviet Astronomy*, 18:691–699, June 1975. [\[ADS\]](#).
- [26] S. Sarkar and A. M. Cooper. Cosmological and experimental constraints on the tau neutrino. *Physics Letters B*, 148:347–354, November 1984. [\[DOI\]](#), [\[ADS\]](#).
- [27] C. Burigana, L. Danese, and G. de Zotti. Formation and evolution of early distortions of the microwave background spectrum - A numerical study. *A&A*, 246:49–58, June 1991. [\[ADS\]](#).
- [28] J. Chluba and R. A. Sunyaev. The evolution of CMB spectral distortions in the early Universe. *MNRAS*, 419:1294–1314, January 2012. [arXiv:1109.6552](#), [\[DOI\]](#), [\[ADS\]](#).
- [29] R. Khatri and R. A. Sunyaev. Beyond  $y$  and  $\mu$ : the shape of the CMB spectral distortions in the intermediate epoch,  $1.5 \times 10^4 \lesssim z \lesssim 2 \times 10^5$ . *JCAP*, 9:016, September 2012. [arXiv:1207.6654](#), [\[DOI\]](#), [\[ADS\]](#).
- [30] J. Chluba. Green’s function of the cosmological thermalization problem. *MNRAS*, 434:352–357, September 2013. [arXiv:1304.6120](#), [\[DOI\]](#), [\[ADS\]](#).
- [31] Sandeep Kumar Acharya and Rishi Khatri. Rich structure of nonthermal relativistic CMB spectral distortions from high energy particle cascades at redshifts  $z \lesssim 2 \times 10^5$ . *Phys.Rev.D*, 99(4):043520, Feb 2019. [arXiv:1808.02897](#), [\[DOI\]](#), [\[ADS\]](#).
- [32] Sandeep Kumar Acharya and Rishi Khatri. New CMB spectral distortion constraints on decaying dark matter with full evolution of electromagnetic cascades before recombination. *Phys.Rev.D*, 99(12):123510, Jun 2019. [arXiv:1903.04503](#), [\[DOI\]](#), [\[ADS\]](#).
- [33] L. Danese and G. de Zotti. Double Compton process and the spectrum of the microwave background. *A&A*, 107:39–42, 1982. [\[ADS\]](#).
- [34] R. Khatri and R. A. Sunyaev. Creation of the CMB spectrum: precise analytic solutions for the blackbody photosphere. *JCAP*, 6:38, 2012. [\[DOI\]](#), [\[ADS\]](#).
- [35] Ia. B. Zeldovich, A. A. Starobinskii, M. Iu. Khlopov, and V. M. Chechetkin. Primordial black holes and the deuterium problem. *Soviet Astronomy Letters*, 3:110–112, June 1977. [\[ADS\]](#).
- [36] J. Ellis, D. V. Nanopoulos, and S. Sarkar. The cosmology of decaying gravitinos. *Nuclear Physics B*, 259:175–188, September 1985. [\[DOI\]](#), [\[ADS\]](#).
- [37] J. Ellis, G. B. Gelmini, J. L. Lopez, D. V. Nanopoulos, and S. Sarkar. Astrophysical constraints on massive unstable neutral relic particles. *Nuclear Physics B*, 373:399–437, April 1992. [\[DOI\]](#), [\[ADS\]](#).
- [38] M. Kawasaki and T. Moroi. Electromagnetic Cascade in the Early Universe and Its Application to the Big Bang Nucleosynthesis. *ApJ*, 452:506, Oct 1995. [arXiv:astro-ph/9412055](#), [\[DOI\]](#), [\[ADS\]](#).

- [39] Masahiro Kawasaki, Kazunori Kohri, Takeo Moroi, and Yoshitaro Takaesu. Revisiting big-bang nucleosynthesis constraints on long-lived decaying particles. *Phys.Rev.D*, 97(2):023502, Jan 2018. [arXiv:1709.01211](#), [\[DOI\]](#), [\[ADS\]](#).
- [40] Vivian Poulin and Pasquale Dario Serpico. Nonuniversal BBN bounds on electromagnetically decaying particles. *Phys.Rev.D*, 91(10):103007, May 2015. [arXiv:1503.04852](#), [\[DOI\]](#), [\[ADS\]](#).
- [41] Marco Hufnagel, Kai Schmidt-Hoberg, and Sebastian Wild. BBN constraints on MeV-scale dark sectors. Part II: Electromagnetic decays. *Journal of Cosmology and Astro-Particle Physics*, 2018(11):032, Nov 2018. [arXiv:1808.09324](#), [\[DOI\]](#), [\[ADS\]](#).
- [42] Lindsay Forestell, David E. Morrissey, and Graham White. Limits from BBN on light electromagnetic decays. *Journal of High Energy Physics*, 2019(1):74, Jan 2019. [arXiv:1809.01179](#), [\[DOI\]](#), [\[ADS\]](#).
- [43] S. W. Hawking. Black hole explosions? *Nature*, 248:30–31, March 1974. [\[DOI\]](#), [\[ADS\]](#).
- [44] S. W. Hawking. Particle creation by black holes. *Communications in Mathematical Physics*, 43:199–220, August 1975. [\[DOI\]](#), [\[ADS\]](#).
- [45] V. Poulin, J. Lesgourgues, and P. D. Serpico. Cosmological constraints on exotic injection of electromagnetic energy. *JCAP*, 3:043, March 2017. [arXiv:1610.10051](#), [\[DOI\]](#), [\[ADS\]](#).
- [46] Steven J. Clark, Bhaskar Dutta, Yu Gao, Louis E. Strigari, and Scott Watson. Planck constraint on relic primordial black holes. *Phys.Rev.D*, 95(8):083006, Apr 2017. [arXiv:1612.07738](#), [\[DOI\]](#), [\[ADS\]](#).
- [47] Patrick Stöcker, Michael Krämer, Julien Lesgourgues, and Vivian Poulin. Exotic energy injection with ExoCLASS: application to the Higgs portal model and evaporating black holes. *JCAP*, 2018(3):018, Mar 2018. [arXiv:1801.01871](#), [\[DOI\]](#), [\[ADS\]](#).
- [48] N. Aghanim et al. Planck 2018 results. VI. Cosmological parameters. *ArXiv e-prints*, July 2018. [arXiv:1807.06209](#), [\[ADS\]](#).
- [49] Tracy R. Slatyer. Indirect dark matter signatures in the cosmic dark ages. II. Ionization, heating, and photon production from arbitrary energy injections. *Phys.Rev.D*, 93(2):023521, Jan 2016. [arXiv:1506.03812](#), [\[DOI\]](#), [\[ADS\]](#).
- [50] Matteo Lucca, Nils Schöneberg, Deanna C. Hooper, Julien Lesgourgues, and Jens Chluba. The synergy between CMB spectral distortions and anisotropies. *arXiv e-prints*, page arXiv:1910.04619, Oct 2019. [arXiv:1910.04619](#), [\[ADS\]](#).
- [51] Harry Poulter, Yacine Ali-Haïmoud, Jan Hamann, Martin White, and Anthony G. Williams. CMB constraints on ultra-light primordial black holes with extended mass distributions. *arXiv e-prints*, page arXiv:1907.06485, Jul 2019. [arXiv:1907.06485](#), [\[ADS\]](#).
- [52] Sandeep Kumar Acharya and Rishi Khatri. CMB anisotropy and BBN constraints on pre-recombination decay of dark matter to visible particles. *JCAP*, 2019(12):046, Dec 2019. [arXiv:1910.06272](#), [\[DOI\]](#), [\[ADS\]](#).
- [53] K. Kohri and Jun’ichi Yokoyama. Primordial black holes and primordial nucleosynthesis: Effects of hadron injection from low mass holes. *Phys.Rev.D*, 61(2):023501, Jan 2000. [arXiv:astro-ph/9908160](#), [\[DOI\]](#), [\[ADS\]](#).
- [54] Steven J. Clark, Bhaskar Dutta, Yu Gao, Yin-Zhe Ma, and Louis E. Strigari. 21 cm limits on

- decaying dark matter and primordial black holes. *Phys.Rev.D*, 98(4):043006, Aug 2018. [arXiv:1803.09390](#), [DOI], [ADS].
- [55] B. J. Carr, Kazunori Kohri, Yuuiti Sendouda, and Jun'ichi Yokoyama. Constraints on primordial black holes from the Galactic gamma-ray background. *Phys.Rev.D*, 94(4):044029, Aug 2016. [arXiv:1604.05349](#), [DOI], [ADS].
- [56] Alexandre Arbey, Jérémy Auffinger, and Joseph Silk. Constraining primordial black hole masses with the isotropic gamma ray background. *arXiv e-prints*, page arXiv:1906.04750, Jun 2019. [arXiv:1906.04750](#), [ADS].
- [57] Mathieu Boudaud and Marco Cirelli. Voyager 1  $e^\pm$  Further Constrain Primordial Black Holes as Dark Matter. *Phys.Rev.Lett*, 122(4):041104, Feb 2019. [arXiv:1807.03075](#), [DOI], [ADS].
- [58] William DeRocco and Peter W. Graham. Constraining primordial black hole abundance with the Galactic 511 keV line. *arXiv e-prints*, page arXiv:1906.07740, Jun 2019. [arXiv:1906.07740](#), [ADS].
- [59] Ranjan Laha. Primordial black holes as a dark matter candidate are severely constrained by the Galactic Center 511 keV gamma-ray line. *arXiv e-prints*, page arXiv:1906.09994, Jun 2019. [arXiv:1906.09994](#), [ADS].
- [60] Basudeb Dasgupta, Ranjan Laha, and Anupam Ray. Neutrino and positron constraints on spinning primordial black hole dark matter. *arXiv e-prints*, page arXiv:1912.01014, Dec 2019. [arXiv:1912.01014](#), [ADS].
- [61] T. Kanzaki and M. Kawasaki. Electron and photon energy deposition in the Universe. *Phys.Rev.D*, 78(10):103004, November 2008. [arXiv:0805.3969](#), [DOI], [ADS].
- [62] T. Kanzaki, M. Kawasaki, and K. Nakayama. Effects of Dark Matter Annihilation on the Cosmic Microwave Background. *Progress of Theoretical Physics*, 123:853–865, May 2010. [arXiv:0907.3985](#), [DOI], [ADS].
- [63] D. N. Page. Particle emission rates from a black hole. II. Massless particles from a rotating hole. *Phys.Rev.D*, 14(12):3260–3273, Dec 1976. [DOI], [ADS].
- [64] D. N. Page. Particle emission rates from a black hole: Massless particles from an uncharged, nonrotating hole. *Phys.Rev.D*, 13:198–206, January 1976. [DOI], [ADS].
- [65] J. H. MacGibbon and B. R. Webber. Quark- and gluon-jet emission from primordial black holes: The instantaneous spectra. *Phys.Rev.D*, 41:3052–3079, May 1990. [DOI], [ADS].
- [66] Tullio Regge and John A. Wheeler. Stability of a Schwarzschild Singularity. *Physical Review*, 108(4):1063–1069, Nov 1957. [DOI], [ADS].
- [67] J. H. MacGibbon. Quark- and gluon-jet emission from primordial black holes. II. The emission over the black-hole lifetime. *Phys.Rev.D*, 44:376–392, July 1991. [DOI], [ADS].
- [68] Tanabashi et. al. Particle Data Group. Review of particle physics. *Phys. Rev. D*, 98:030001, Aug 2018. URL: <https://link.aps.org/doi/10.1103/PhysRevD.98.030001>, [DOI].
- [69] Torbjörn Sjöstrand, Stephen Mrenna, and Peter Skands. PYTHIA 6.4 physics and manual. *Journal of High Energy Physics*, 2006(5):026, May 2006. [arXiv:hep-ph/0603175](#), [DOI], [ADS].

- [70] Torbjörn Sjöstrand, Stefan Ask, Jesper R. Christiansen, Richard Corke, Nishita Desai, Philip Ilten, Stephen Mrenna, Stefan Prestel, Christine O. Rasmussen, and Peter Z. Skands. An introduction to PYTHIA 8.2. *Computer Physics Communications*, 191:159–177, Jun 2015. [arXiv:1410.3012](#), [DOI], [ADS].
- [71] S. Seager, D. D. Sasselov, and D. Scott. A New Calculation of the Recombination Epoch. *ApJL*, 523:L1–L5, September 1999. [arXiv:astro-ph/9909275](#), [DOI], [ADS].
- [72] J. Chluba and R. M. Thomas. Towards a complete treatment of the cosmological recombination problem. *MNRAS*, 412:748–764, April 2011. [arXiv:1010.3631](#), [DOI], [ADS].
- [73] J. Chluba and R. A. Sunyaev. Induced two-photon decay of the 2s level and the rate of cosmological hydrogen recombination. *A&A*, 446:39–42, January 2006. [arXiv:astro-ph/0508144](#), [DOI], [ADS].
- [74] Eric R. Switzer and Christopher M. Hirata. Primordial helium recombination. I. Feedback, line transfer, and continuum opacity. *Phys.Rev.D*, 77(8):083006, Apr 2008. [arXiv:astro-ph/0702143](#), [DOI], [ADS].
- [75] J. A. Rubiño-Martín, J. Chluba, and R. A. Sunyaev. Lines in the cosmic microwave background spectrum from the epoch of cosmological helium recombination. *A&A*, 485(2):377–393, Jul 2008. [arXiv:0711.0594](#), [DOI], [ADS].
- [76] Daniel Grin and Christopher M. Hirata. Cosmological hydrogen recombination: The effect of extremely high-n states. *Phys.Rev.D*, 81(8):083005, Apr 2010. [arXiv:0911.1359](#), [DOI], [ADS].
- [77] J. Chluba, G. M. Vasil, and L. J. Dursi. Recombinations to the Rydberg states of hydrogen and their effect during the cosmological recombination epoch. *MNRAS*, 407(1):599–612, Sep 2010. [arXiv:1003.4928](#), [DOI], [ADS].
- [78] Yacine Ali-Haïmoud and Christopher M. Hirata. Ultrafast effective multilevel atom method for primordial hydrogen recombination. *Phys.Rev.D*, 82(6):063521, Sep 2010. [arXiv:1006.1355](#), [DOI], [ADS].
- [79] Y. Ali-Haïmoud and C. M. Hirata. HyRec: A fast and highly accurate primordial hydrogen and helium recombination code. *Phys.Rev.D*, 83(4):043513, February 2011. [arXiv:1011.3758](#), [DOI], [ADS].
- [80] Sandeep Kumar Acharya and Rishi Khatri. CMB spectral distortions constraints on primordial black holes, cosmic strings and long lived unstable particles revisited. *arXiv e-prints*, page arXiv:1912.10995, Dec 2019. [arXiv:1912.10995](#), [ADS].
- [81] D. J. Fixsen, E. S. Cheng, J. M. Gales, J. C. Mather, R. A. Shafer, and E. L. Wright. The Cosmic Microwave Background Spectrum from the Full COBE FIRAS Data Set. *ApJ*, 473:576, December 1996. [arXiv:astro-ph/9605054](#), [DOI], [ADS].
- [82] D. J. Fixsen and J. C. Mather. The Spectral Results of the Far-Infrared Absolute Spectrophotometer Instrument on COBE. *ApJ*, 581:817–822, December 2002. [DOI], [ADS].
- [83] A. Kogut, D. J. Fixsen, D. T. Chuss, J. Dotson, E. Dwek, M. Halpern, G. F. Hinshaw, S. M. Meyer, S. H. Moseley, M. D. Seiffert, D. N. Spergel, and E. J. Wollack. The Primordial Inflation Explorer (PIXIE): a nulling polarimeter for cosmic microwave background observations. *JCAP*, 7:025, July 2011. [arXiv:1105.2044](#), [DOI], [ADS].

- [84] Antony Lewis and Sarah Bridle. Cosmological parameters from CMB and other data: A Monte Carlo approach. *Phys.Rev.D*, 66(10):103511, Nov 2002. [arXiv:astro-ph/0205436](#), [DOI], [ADS].
- [85] Planck Collaboration. Planck 2018 results. V. CMB power spectra and likelihoods. *arXiv e-prints*, page arXiv:1907.12875, July 2019. [arXiv:1907.12875](#), [ADS].
- [86] T. M. Bania, Robert T. Rood, and Dana S. Balser. The cosmological density of baryons from observations of 3He+ in the Milky Way. *Nature*, 415, 2002. [DOI].
- [87] J. D. Bowman, A. E. E. Rogers, R. A. Monslave, T. J. Mozdzen, and N. Mahesh. An absorption profile centred at 78 megahertz in the sky-averaged spectrum. *Nature*, 555, 2018. [DOI].
- [88] G. F. Chapline. Cosmological effects of primordial black holes. *Nature*, 253(5489):251–252, Jan 1975. [DOI], [ADS].
- [89] B. J. Carr, J. H. Gilbert, and James E. Lidsey. Black hole relics and inflation: Limits on blue perturbation spectra. *Phys.Rev.D*, 50(8):4853–4867, Oct 1994. [arXiv:astro-ph/9405027](#), [DOI], [ADS].
- [90] P. Ivanov, P. Naselsky, and I. Novikov. Inflation and primordial black holes as dark matter. *Phys.Rev.D*, 50(12):7173–7178, Dec 1994. [DOI], [ADS].
- [91] Amandeep S. Josan, Anne M. Green, and Karim A. Malik. Generalized constraints on the curvature perturbation from primordial black holes. *Phys.Rev.D*, 79(10):103520, May 2009. [arXiv:0903.3184](#), [DOI], [ADS].
- [92] Gabriela Sato-Polito, Ely D. Kovetz, and Marc Kamionkowski. Constraints on the primordial curvature power spectrum from primordial black holes. *Phys.Rev.D*, 100(6):063521, Sep 2019. [arXiv:1904.10971](#), [DOI], [ADS].
- [93] Tomohiro Harada, Chul-Moon Yoo, and Kazunori Kohri. Threshold of primordial black hole formation. *Phys.Rev.D*, 88(8):084051, Oct 2013. [arXiv:1309.4201](#), [DOI], [ADS].
- [94] Albert Escrivà, Cristiano Germani, and Ravi K. Sheth. Universal threshold for primordial black hole formation. *Phys.Rev.D*, 101(4):044022, February 2020. [arXiv:1907.13311](#), [DOI], [ADS].
- [95] Anne M. Green, Andrew R. Liddle, Karim A. Malik, and Misao Sasaki. New calculation of the mass fraction of primordial black holes. *Phys.Rev.D*, 70(4):041502, Aug 2004. [arXiv:astro-ph/0403181](#), [DOI], [ADS].
- [96] Rishi Khatri and Rashid A. Sunyaev. Forecasts for CMB  $\mu$  and i-type spectral distortion constraints on the primordial power spectrum on scales  $8\text{less}sim\text{kless}sim10^4 \text{ Mpc}^{-1}$  with the future Pixie-like experiments. *Journal of Cosmology and Astro-Particle Physics*, 2013(6):026, Jun 2013. [arXiv:1303.7212](#), [DOI], [ADS].
- [97] Aghanim et. al. Planck Collaboration. Planck 2015 results. XI. CMB power spectra, likelihoods, and robustness of parameters. *A&A*, 594:A11, Sep 2016. [arXiv:1507.02704](#), [DOI], [ADS].

## A Comparison of CMB constraints from Planck 2015 and 2018 data

**Table 1:** Comparison of constraints on abundance of black hole  $f_{\text{BH}}$  from Planck 2015 [97] and Planck 2018 [85] data for monochromatic black hole mass function.

$M_{\text{BH},0}$ (g)	P2015	P2018
$1.1 \times 10^{13}$	$3.92 \times 10^{-4}$	$3.05 \times 10^{-4}$
$1.2 \times 10^{13}$	$1.81 \times 10^{-5}$	$1.78 \times 10^{-5}$
$1.5 \times 10^{13}$	$6.48 \times 10^{-8}$	$5.32 \times 10^{-8}$
$2 \times 10^{13}$	$6.53 \times 10^{-10}$	$5.36 \times 10^{-10}$
$2.5 \times 10^{13}$	$7.62 \times 10^{-11}$	$5.31 \times 10^{-11}$
$4 \times 10^{13}$	$9.4 \times 10^{-11}$	$9.1 \times 10^{-11}$
$10^{14}$	$5 \times 10^{-9}$	$4.36 \times 10^{-9}$
$10^{15}$	$2.7 \times 10^{-6}$	$2.58 \times 10^{-6}$
$10^{16}$	$2.62 \times 10^{-3}$	$2.54 \times 10^{-3}$
$2 \times 10^{16}$	$3.56 \times 10^{-2}$	$3.2 \times 10^{-2}$
$5 \times 10^{16}$	2.16	1.94